ISSN 1674-1056
http://cpb.iphy.ac.cn
http://iopscience.iop.org/cpb
中国物理 B
Chinese Physics
中国物理
Chinese Physics B

Thermomechanical response of aluminum alloys under the combined action of tensile loading and laser irradiations

Mohsan Jelani, Zewen Li(李泽文), Zhonghua Shen(沈中华), Maryam Sardar
Citation: Chin. Phys. B . 2018, 27(3): 037901. **doi:** 10.1088/1674-1056/27/3/037901

Journal homepage: http://cpb.iphy.ac.cn; http://iopscience.iop.org/cpb

What follows is a list of articles you may be interested in

Influence of secondary treatment with CO_2 laser irradiation for mitigation site on fused silica surface

Yong Jiang(蒋勇), Qiang Zhou(周强), Rong Qiu(邱荣), Xiang Gao(高翔), Hui-Li Wang(王慧丽), Cai-Zhen Yao(姚彩珍), Jun-Bo Wang(王俊波), Xin Zhao(赵鑫), Chun-Ming Liu(刘春明), Xia Xiang(向霞), Xiao-Tao Zu(祖小涛), Xiao-Dong Yuan(袁晓东), Xin-Xiang Miao(苗心向)
Chin. Phys. B . 2016, 25(10): 108104. **doi:** 10.1088/1674-1056/25/10/108104

Effects of twin and stacking faults on the deformation behaviors of Al nanowires under tension loading

An Min-Rong, Song Hai-Yang, Su Jin-Fang
Chin. Phys. B . 2012, 21(10): 106202. **doi:** 10.1088/1674-1056/21/10/106202

Elastic properties of Nb-based alloys by using the density functional theory

Liu Zeng-Hui, Shang Jia-Xiang
Chin. Phys. B . 2012, 21(1): 016202. **doi:** 10.1088/1674-1056/21/1/016202

Thermomechanical response of aluminum alloys under the combined action of tensile loading and laser irradiations*

Mohsan Jelani[1], Zewen Li (李泽文)[2,†], Zhonghua Shen(沈中华)[1,2], and Maryam Sardar[1]

[1] School of Science, Nanjing University of Science and Technology, Nanjing 210094, China
[2] Advanced Launching Co-Innovation Centre, Nanjing University of Science and Technology, Nanjing 210094, China

(Received 7 September 2017; revised manuscript received 15 December 2017; published online 13 February 2018)

This study reports the investigation of the thermomechanical behavior of aluminum alloys (Al-1060, Al-6061, and Al-7075) under the combined action of tensile loading and laser irradiations. The continuous wave ytterbium fiber laser (wavelength 1080 nm) was employed as the irradiation source, while tensile loading was provided by the tensile testing machine. The effects of various pre-loading and laser power densities on the failure time, temperature distribution, and the deformation behavior of aluminum alloys are analyzed. The experimental results represent the significant reduction in failure time for higher laser power densities and for high preloading values, which implies that preloading may contribute a significant role in the failure of the material at elevated temperature. Fracture on a microscopic scale was predominantly ductile comprising micro-void nucleation, growth, and coalescence. The Al-1060 specimens behaved plastically to some extent, while Al-6061 and Al-7075 specimens experienced catastrophic failure. The reason and characterization of material failure by tensile and laser loading are explored in detail. A comparative behavior of under-tested materials is also investigated. This work suggests that studies considering only combined loading are not enough to fully understand the mechanical behavior of under-tested materials. For complete characterization, one should consider the effect of heating as well as loading rate and the corresponding involved processes with the help of thermomechanical coupling and the thermal elastic-plastic theory.

Keywords: aluminum alloys, fiber laser, tensile loading, thermomechanical effects, failure evolution

PACS: 79.20.Ds, 81.40.Wx, 81.70.Bt, 62.20.M– **DOI:** 10.1088/1674-1056/27/3/037901

1. Introduction

Aluminum alloys, because of their high strength to weight ratio, mechanical stability, thermal management, ease of fabrication, machining, and ability to withstand the stresses that occur during launch and operation, have been used as the primary structural material for the automotive and aeronautic industries.[1–5] In aerospace engineering, various structural components may be subjected to severe thermal loading, which may be originated by aerodynamic heating, laser irradiation, or local intense fire. Besides aerospace engineering, aluminum alloys are increasingly being employed in a broad range of load bearing applications, such as lightweight structures, light rail, bridge decks, marine crafts, and offshore platforms. The aluminum alloy's applications in a preloaded environment demand for a more detailed investigation to its thermomechanical behavior for determining the safety of materials, designing components, and service performance assessment.[6]

High energy, continuous wave lasers are a proficient source of varying levels of machining or damaging to structural materials. Studies about the laser damage effect of aluminum, focusing on continuous laser[7–10] as well as high pulse laser,[11–15] were carried out frequently during the past several decades. However, the research about the laser damage effect of aluminum under preloaded conditions is infrequent and should be considered. The combined laser beam and mechanical loading may significantly reduce the breakdown time, energy, and room temperature tensile strength.[9,16] This may also help to avoid the material melting and being burn through before breakdown due to strong local thermal inconsistency. The combination of laser energy with mechanical loading remarkably increases micro defects of the material and degrade the mechanical properties of the specimen. In subject to the presented issue, a brief review of some studies on structural materials considering preload and laser irradiation is illustrated below.

Medford *et al.*[9] developed an analytical model to determine failure threshold and to predict the thermal and structural response of aluminum alloys under combined effects of laser beam exposure and mechanical loading. The specimens were irradiated by continuous wave (CW) CO_2 laser under tension or compression in the presence of tangential subsonic flow. It was observed that combined laser exposure and mechanical loading significantly reduced the room temperature tensile strength and threshold energy. Yang *et al.*[16] studied experimentally the CW laser damage effect on steel under preloaded invariable stretching stress. The 30CrMnSiA steel sample was

*Project supported by the National Natural Science Foundation of China (Grant No. 61605079) and the Fundamental Research Funds for the Central Universities, China (Grant No. 30916014112-020).

†Corresponding author. E-mail: lizewen@njust.edu.cn

© 2018 Chinese Physical Society and IOP Publishing Ltd

preloaded with invariable stretching force and then irradiated by YAG laser. An empirical formula was derived, which relates the stretching stress and rupture temperature. Moreover, a decrease in threshold rupture laser energy with the increase of stretching stress or laser power density was reported. Long *et al.*[17] presented the effects of laser power density, preloading, and the thickness on the failure time of the carbon fibre/epoxy composite laminates subjected to CW CO_2 laser.

The current work focuses on the experimental investigations of the thermomechanical behavior of aluminum alloys subjected to combined tensile loading and laser irradiation. The purpose of the laser damaging is to determine the laser power density required to significantly change the structural capability of the under-tested materials and to explore the dependency of specimens' failure time and failure temperature on preload and laser power density. Moreover, we aim to investigate the comparative response of different types of aluminum alloys under simultaneous tensile loading and laser heating. To explore these objectives, three types of aluminum alloys (Al-1060, Al-6061, and Al-7075) were exposed to simultaneous tensile loading and CW ytterbium fiber laser irradiations. The temperature rise, deformation behavior, and failure time were recorded by using a pyrometer and high-speed video camera, respectively. The fractured surfaces of the specimens after tensile tests were examined through scanning electron microscopy.

2. Experimental detail

Three different kinds of aluminum alloys (Al-1060, Al-6061, and Al-7075) were used for the experiments in this investigation. The rectangularly shaped samples with the length of 150 mm, the width of 10 mm, and the thickness of 2 mm were selected. The specimens were prepared in the sufficient length (80 mm gauge length) to ensure a region about the center in which the temperature does not vary much along the length. Moreover, in the normal tensile testing, the standard test sample (machined into a reduced section or in dog bone shape) is required to avoid fracture in the grips. In our case, since the gripped portion of the test specimen (heated by laser) is much cooler than the central part, a transition section is not required to avoid fracture in the gripped sections. The chemical composition and physical properties of the used materials are given in Table 1 and Table 2, respectively.

Table 1. The chemical composition of aluminum alloys in weight %.

Alloy	Cu	Fe	Mg	Zn	Mn	Si	Al
Al-1060	0.05	0.35	0.03	0.05	0.03	0.25	balance
Al-6061	0.4	0.7	1.2	0.25	0.15	0.8	balance
Al-7075	1.6	0.5	2.5	6.1	0.3	0.4	balance

Table 2. The physical and mechanical properties of the under-tested materials.[18–20]

Physical properties	Al-1060	Al-6061	Al-7075
Room temperature ultimate tensile strength/MPa	115	403	605
Room temperature tensile yield strength/MPa	115	370	565
Density/g·cm^{-3}	2.7	2.7	2.8
Melting point/°C	646–657	582–652	477–635
Thermal conductivity/W·m^{-1}·K^{-1}	234	173	130
Thermal diffusivity/mm^2·s^{-1}	95	70	46
Strength/weight/kN·m·kg^{-1}	26–48	48–144	86–211
Specific heat capacity/J·kg^{-1}·K^{-1}	896	900	910

Before carrying out the experiments, the room temperature tensile strength of specimens was measured by using the JVJ-50S universal testing machine. The measured values of room temperature tensile strengths are 115, 403, and 605 MPa for Al-1060, Al-6061, and Al-7075 alloys, respectively.

The experiments were conducted for four different load values, including 40%, 55%, 70%, and 85% of room temperature tensile strengths. The actual values of preloaded stress are listed in Table 3. The loading was provided by a JVJ-50S universal testing machine with a crosshead speed (loading rate) of 3 mm/min.

The continuous wave ytterbium (Yb) fiber laser RFL-C1000 was employed for laser loading. The maximum power of the laser system is 1 kW with wavelength 1080 nm. The distance between the laser emitter and the specimen was 60 cm. The laser spot that was 7 mm in diameter was perpendicularly focused on the center of the specimen, with four laser powers 55, 70, 85, and 100% of the maximum power of the laser system used in the test. The corresponding laser power densities are calculated and given in Table 3. The samples were divided into three groups based on material type. The laser began to irradiate when the measured pre-load reached the predetermined value. The specimens were continuously irradiated until failure occurred and the exposure time required for complete failure was recorded. All the process was observed and recorded simultaneously with a high-speed video camera and by the pyrometer (see Fig. 1). The fracture surfaces (within thickness) or metallographs of the specimens after tensile tests were examined through scanning electron microscopy (SEM, FEI Quanta 250F).

Table 3. Experimental parameters: laser power densities and tensile loading values.

Material type	Sample number	Laser power densities/kW·cm^{-2}	Pre-load/MPa
Al-1060	1–4	1.5, 1.9, 2.3, 2.7 (In order, one for every 4 samples)	97
	5–8		80
	9–12		63
	13–16		46
Al-6061	17–20		342
	21–24		282
	25–28		222
	29–32		161
Al-7075	33–36		514
	37–40		423
	41–44		333
	45–48		242

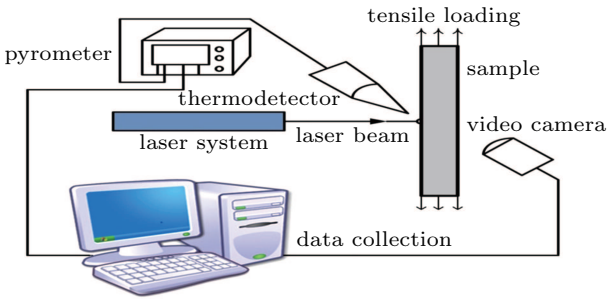


Fig. 1. (color online) Experimental setup for laser irradiation of preloaded specimen.

3. Results and discussion

3.1. Strength degradation

Figure 2 represents the failure behavior as a function of pre-loaded values under fixed laser power densities for the Al-1060 type specimens. For the laser power density of 1.5 kW/cm^2, as the laser starts to irradiation, the tensile stress drops dramatically due to thermal expansion. At some point the tensile stress increases again because the loading overcomes the thermal expansion and tries to recover to the preloaded value, and forms a valley. Here, the highest point of the stress curve after the valley is called the yield point, beyond which the flow stress continually decreases until specimen's fracture. It is important to note that firstly the load applied to the specimen is not constant in the process and secondly the yield point is not constant, with a changing inhomogeneous temperature field in the specimen. Therefore, the definition and determination of the yielding of the specimen is unusual. When the stress increases to the yield point of the samples, it decreases again and at some point drops dramatically until the samples complete failure due to the sample fracture, as shown in Fig. 2(a) line 1. With the increase of pre-loaded value, the depth of the valley decreases and even disappears for the higher pre-loaded values, as shown in Fig. 2(a) line 4.

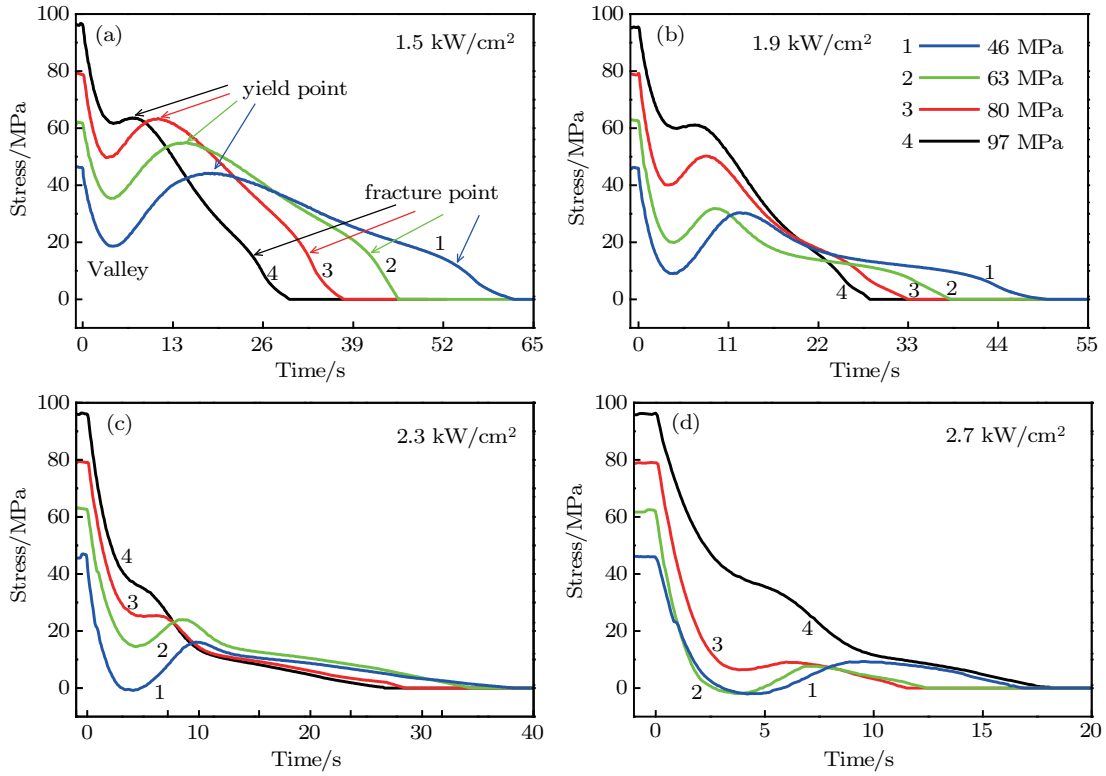


Fig. 2. (color online) Failure behavior of the Al-1060 specimens as a function of pre-loaded values under fixed laser power densities: (a) 1.5 kW/cm^2, (b) 1.9 kW/cm^2, (c) 2.3 kW/cm^2, and (d) 2.7 kW/cm^2.

When the samples took comparatively shorter time to reach the the yield point, which means that the temperature is lower at the yield point, so the yield point value increases along with the preloaded value. At last, the samples also took comparatively shorter time to reach the complete failure. For the laser power density of 1.9 kW/cm^2, the sample showed similar behavior as that of 1.5 kW/cm^2. For higher power densities 2.3 kW/cm^2 and 2.7 kW/cm^2, the thermal effects start to dominate on the preloading effect and even predominate on the loading effect, the tensile stress shows negative under lower load values, and the fracture point disappears.

Figure 3 demonstrates the failure behavior as a function of laser power densities under fixed pre-loaded values for the Al-1060 type specimens. Under lower preloaded conditions of 46 MPa and 63 MPa, the depth of the valley increases along with the increasing laser power density due to faster thermal expansion. Meanwhile, the samples took a comparatively shorter time to reach the yield point and with a lower yield point value, which means that the temperature is higher at the yield point, so the yield point value decreases along with the increasing laser power density. At last, the samples also took comparatively shorter time to reach the complete failure. Under higher preloaded conditions of 80 MPa, with the increase of laser power density, the specimen experienced comparatively enhanced thermal effects and the valley disappeared at 2.3 kW/cm^2. For higher loading and higher laser density, the behavior is almost the same. So for 97 MPa preloading, the behavior showed a few differences.

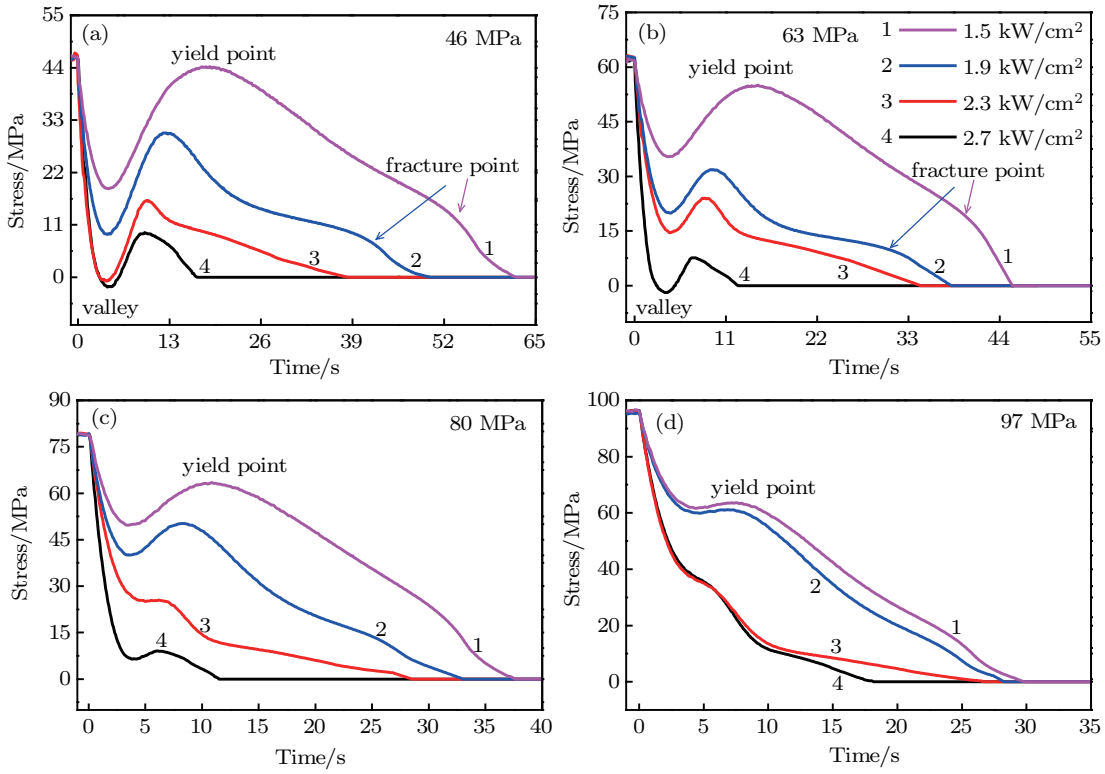


Fig. 3. (color online) Failure behavior of Al-1060 specimens for various laser power densities under the fixed preloading conditions: (a) 46 MPa, (b) 63 MPa, (c) 80 MPa, and (d) 97 MPa.

Figure 4 represents the failure behavior of Al-7075 specimens subjected to various preloading under the fixed laser power densities. In Fig. 4(a) for 1.5 kW/cm^2, under 242 MPa preload, as the laser starts, the tensile stress decreases due to thermal expansion, but the Al-7075 is more brittle and anti-temperature, so the decease is comparatively little. After that, the preloading and the thermal expansion equally contribute to the deformation.

As the laser continually irradiates, the temperature rises, and at some point the tensile stress decreases faster due to the yield stress level shown out. After a while at some point, the tensile stress decreases most sharply due to the fracture point achievement, until the fracture is complete and the tensile stress falls to zero.

As the preloading value increased, specimen took a shorter time to reach the yield point, fracture point, and complete failure but with higher yield point value and fracture point value. Meanwhile, for higher preloading values of 423 MPa and 514 MPa, the fracture process was relatively fast. For the higher power densities 1.9 kW/cm^2 in Fig. 4(b), a similar behavior as that of 1.5 kW/cm^2 is observed. For 2.3 kW/cm^2 and 2.7 kW/cm^2 in Figs. 4(c) and 4(d), under the lower preloads the fracture becomes weak and the fracture point is unobvious due to plastic deformation occurrence owing to the higher laser power density and elevated temperature.

Figure 5 represents the failure behavior of Al-7075 specimens subjected to various laser power densities under the fixed preloading conditions. In Fig. 5(a), it shows that as the increasing laser power density, the yield point, the fracture point, and the complete failure decrease due to relatively high-temperature rise. Figures 5(b) and 5(c) show similar behavior for all specimens with significant shortening in failure time with the increase of power densities. For the highest preloaded condition in Fig. 5(d), relatively quicker failure is observed with the increase of laser power densities.

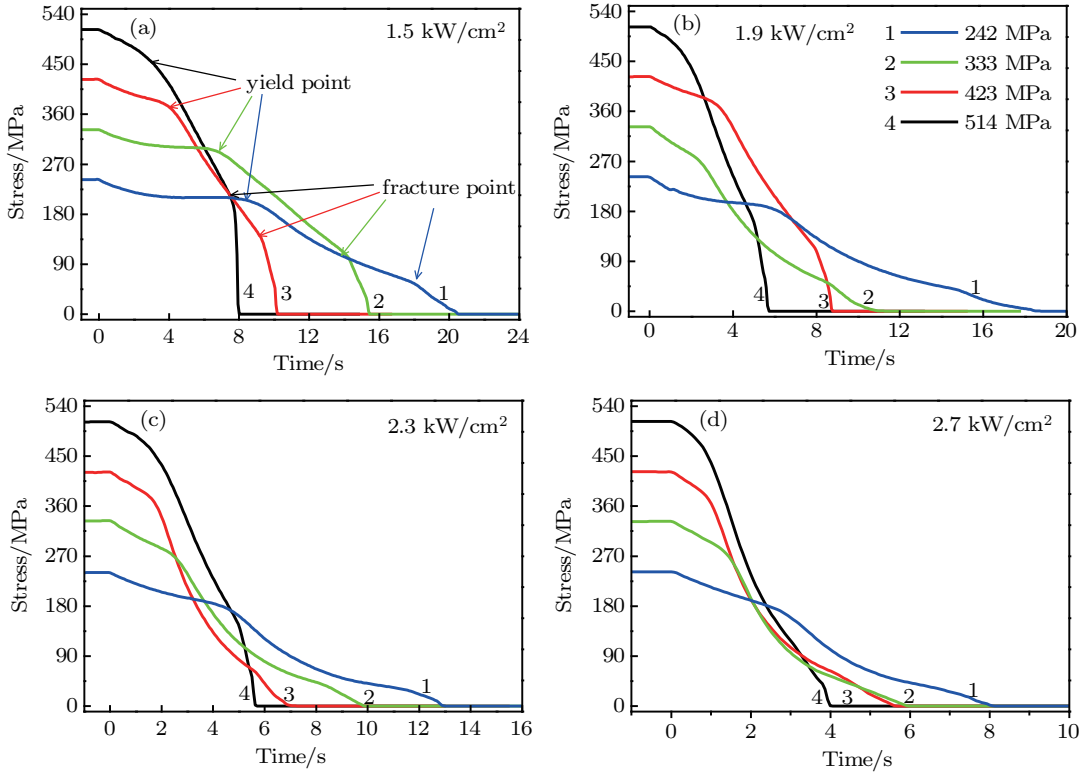


Fig. 4. (color online) Failure behavior of the Al-7075 specimens as a function of pre-loaded values under fixed laser power densities: (a) 1.5 kW/cm^2, (b) 1.9 kW/cm^2, (c) 2.3 kW/cm^2, and (d) 2.7 kW/cm^2.

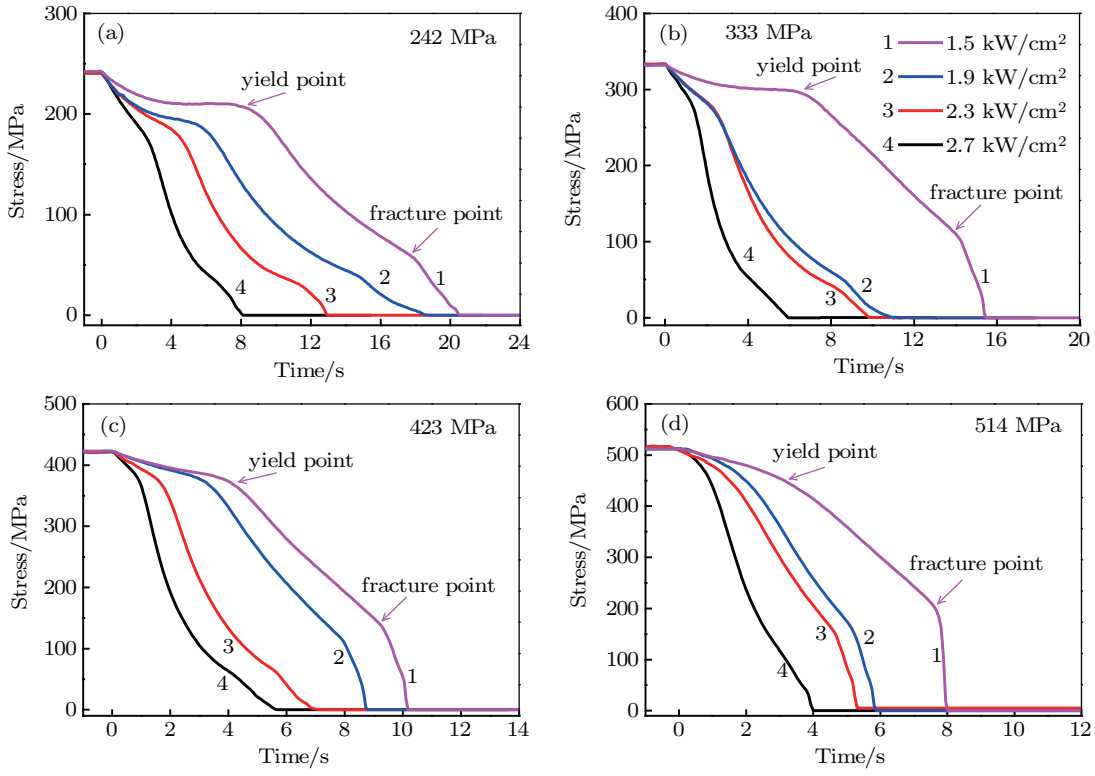


Fig. 5. (color online) Failure behavior of Al-7075 specimens for various laser power densities under the fixed preloading conditions: (a) 242 MPa, (b) 333 MPa, (c) 423 MPa, and (d) 514 MPa.

For Al-6061 type specimens, the failure behavior with respect to laser power densities and preloads is included in our previous work.[21] It was observed that the Al-6061 specimen's deformation pattern is almost the same as that of Al-7075 specimens. Since the Al-6061 is more brittle and with higher strength, the decrease in yield stress with the increase of power density or preload is fewer than Al-1060 specimens. But there is no significant difference as compared to Al-7075. For higher power densities/preload, the fracture point becomes weak, because relatively higher elevated temperature induced by the higher laser power density makes the material plasticity dominant.

3.2. Failure time

Figure 6 represents the failure time (the time from the start of laser irradiation to the fracture of the specimen) as a function of preload and laser power density respectively for the Al-1060 type specimens.

In Fig. 6(a), the failure time decreased along with increasing power density at the same preload. The preloading influence on shortening the failure time is significant under low load values with the increase of power density. For maximum loading of 97 MPa, very slight decrease in failure time with increasing power density is observed. Figure 6(b) represents the overall decrease in the failure time with the increase of pre-loaded values except in the case of highest laser power density. The influence of preloading on failure time reduction is more significant for low laser power densities with higher preload values. For 1.5 kW/cm^2 and 1.9 kW/cm^2 laser power densities, preloading reduces failure time significantly, but for higher laser power density of 2.3 kW/cm^2, preloading effects start to be dominated by thermal effects. For the maximum laser power density of 2.7 kW/cm^2, these effects are more considerable, therefore the failure time increases slightly instead of decreasing. The possible reason is that the higher preloading with higher power density offers more capability for thermal expansion.

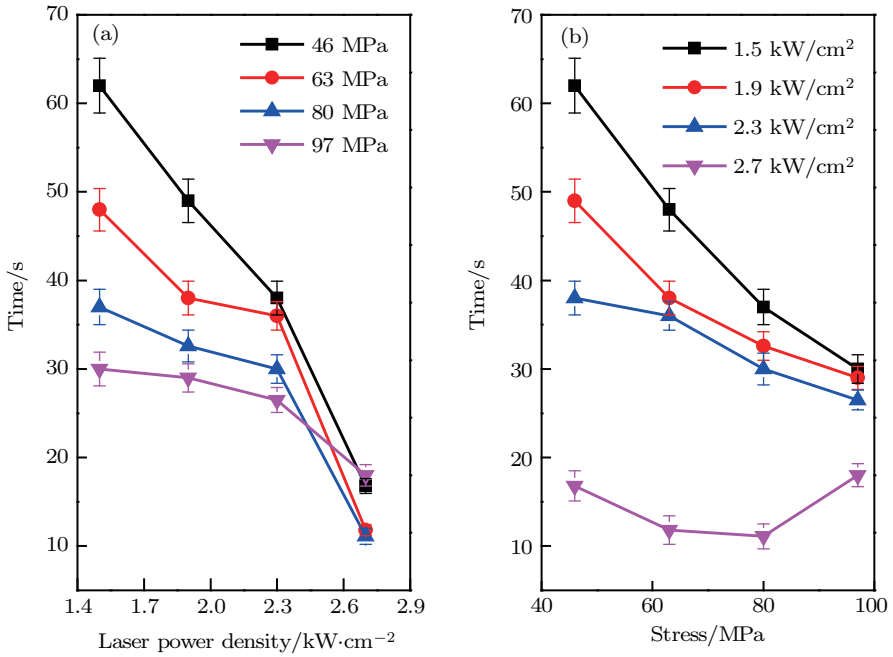


Fig. 6. (color online) Failure time variation for Al-1060 specimens subjected to various laser power densities and preloading. (a) Time versus laser power density for various preloads. (b) Time versus preload for various laser power densities.

Figure 7 represents the variation of failure time under fixed laser power and fixed tensile preloading respectively for Al-7075 type specimens. Figure 7(a) shows the decrease of failure time with the increase of laser power densities, which is more obvious in the case of lower preload values. A similar trend as that of Al-6061 specimens in the failure time reduction with increasing preload and laser power is noticed.[21] Under 242 MPa loading, with the increase of power density, a large reduction in failure time is found. For 333 MPa preload, when the power density increases from 1.5 to 1.9 kW/cm^2, a notable decrease in failure time is observed, but for further increase in power density, the decreasing rate becomes slow and small. For the case of 423 MPa preload, with the increase of power density, a small and linear reduction in failure time is observed.

Under the condition of 514 MPa preload, initially, failure time reduces with the increase of power density from 1.5 to 1.9 kW/cm^2. A slight increase in failure time is observed when the power density increases to 2.3 kW/cm^2, but for the maximum power density of 2.7 kW/cm^2, again failure time decreases. In Fig. 7(b), overall decreasing trend in failure time with the increase of preloading is observed. For the lower

power densities of 1.5 and 1.9 kW/cm^2, with the increase of preload, a significant decrease in failure time is observed. For higher power densities of 2.3 and 2.7 kW/cm^2, a relatively small difference in failure time with increasing preload is found.

For Al-6061 specimens, failure time variation as a function of laser power density and preload is included in our previous work.[21] Those results illustrate the overall decrease of failure time with the increase of laser power densities or preloading. However, the decreasing capacity is limited to low preload and low laser power densities. For the higher laser power densities of 2.73 kW/cm^2 and 2.7 kW/cm^2, with the increase of preload, only slight or no reduction in failure time is found. In summary, for the case of Al-6061 specimens, preloading contributes significantly to reducing the failure time of specimens under low laser power densities.

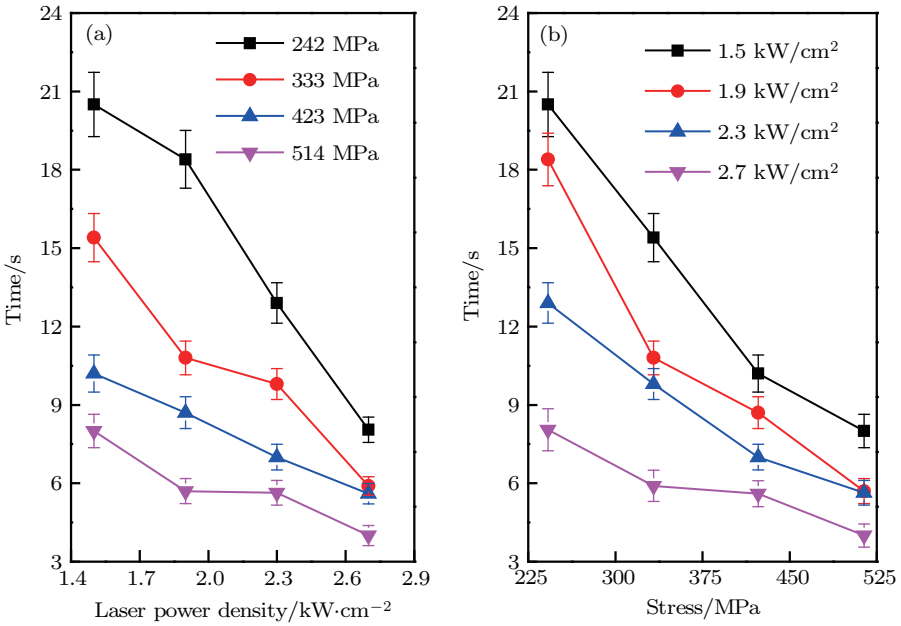


Fig. 7. (color online) Failure time variation for Al-7075 specimens subjected to various laser power densities and preloading. (a) Time versus laser power density for various preloads. (b) Time versus preload for various laser power densities.

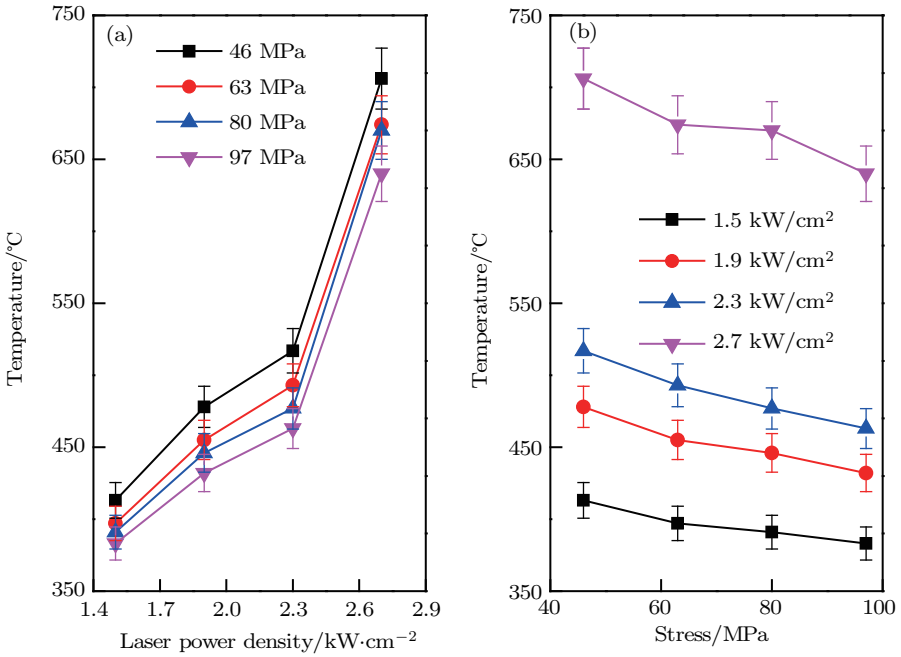


Fig. 8. (color online) Failure temperature variation for Al-1060 specimens subjected to various laser power densities and preloading. (a) Temperature versus laser power density for various preloads. (b) Temperature versus preload for various laser power densities.

3.3. Failure temperature

Figure 8 expresses the failure temperature (the temperature of the center point of the front surface of the specimen when it gets fractured and laser irradiation is turned off) of Al-1060 as a function of preload and laser power density, respectively.

Figures 9 and 10 give the failure temperature of Al-7075 and Al-6061 type specimens as a function of preload and laser power density, respectively.

From Figs. 8–10, it is observed that, for all kinds of specimens with a fixed load value, the temperature rise rate increases and becomes sharp with time by the increase of laser power density. Moreover, for the fixed laser power density, the temperature rise rate decreases with the increase of preload value. For the higher laser power densities, especially for 2.7 kW/cm^2, the rise in failure temperature is relatively high. The rise in temperature in the laser irradiated area is credited to absorption of laser energy which causes the decrease of the material strength, thermal expansion, and local combustion melting.

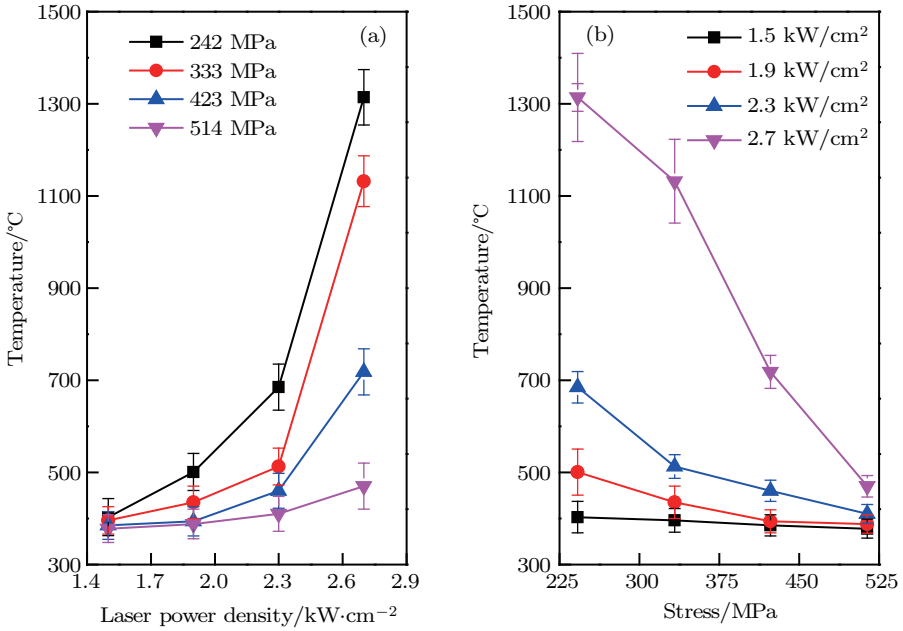


Fig. 9. (color online) Failure temperature variation for Al-7075 specimens subjected to various laser power densities and preloading. (a) Temperature versus laser power density for various preloads. (b) Temperature versus preload for various laser power densities.

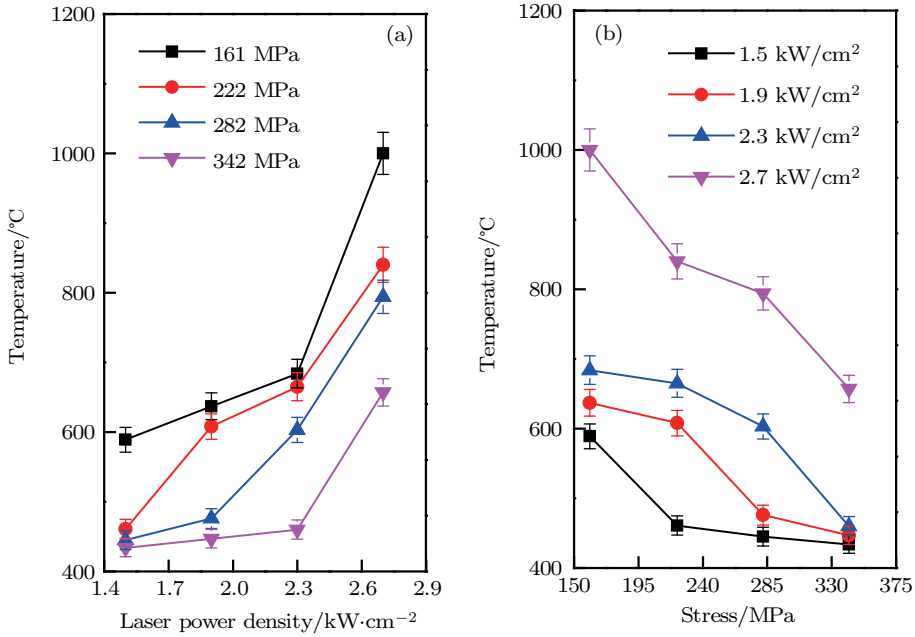


Fig. 10. (color online) Failure temperature variation for Al-6061 specimens subjected to various laser power densities and preloading. (a) Temperature versus laser power density for various preloads. (b) Temperature versus preload for various laser power densities.

The combined effect of tensile load and thermal effects gradually accelerated the crack initiation and expansion, and caused complete failure of specimens. It is observed that for most of the specimens under the fixed laser power density, the failure temperature of the pre-loaded material reduces with the increase of pre-loaded stress, due to the softening (tensile strength reduces) of material at elevated temperature.[22,23]

In general, higher laser power densities under fixed preloading exhibit the distinct rise in maximum temperature. The remarkable reduction in failure temperature can be observed with the increase of pre-loaded values, which implies that preloading may contribute a significant role in the failure of the material at elevated temperature. Especially, in the case of higher laser power densities, the difference between the failure temperatures with increasing pre-load is significant and the effect of preloading becomes dominant, which can be observed by comparing the curves corresponding to 2.7 kW/cm^2 laser power density for all kinds of tested specimens. When we compare the temperature rise rate for the three under-tested materials, it is found that, in general, with the increase of laser power density, the temperature rise rate and the maximum value of temperature rise for Al-6061 are highest and least for Al-7075 except for the maximum laser power density. The comparatively low temperature rise in Al-7075 is attributed to the relative increase of micro defects in the preloaded material due to local thermal inconsistency owing to the relatively low thermal conductivity value.

3.4. Rupture morphology

The difference in the rupture morphology under different preloading stress conditions for the maximum and minimum employed laser power densities is shown in Fig. 11.

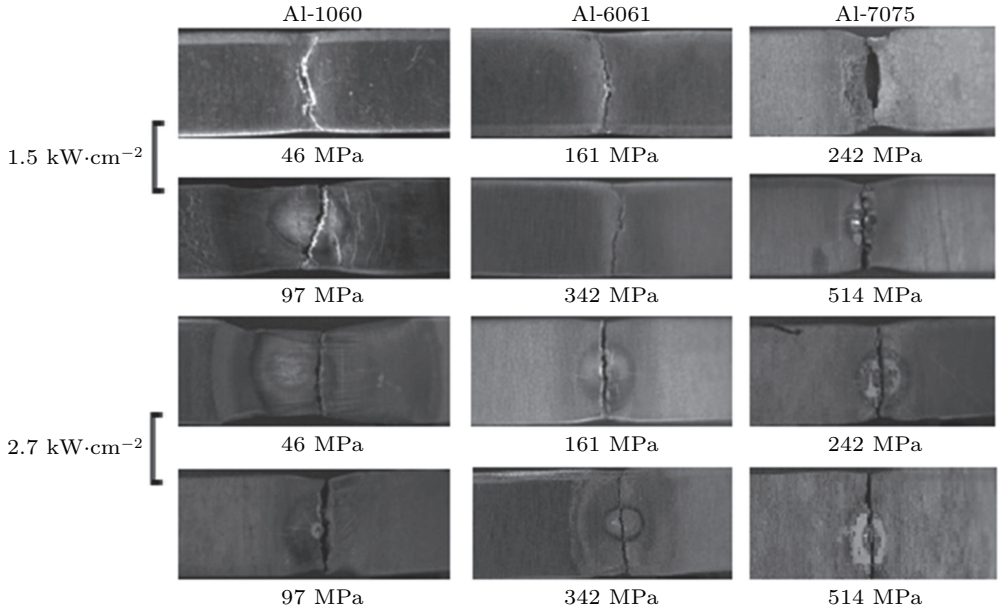


Fig. 11. Rupture texture of the specimens fractured by different preloading stress while the laser power densities are 1.5 kW/cm^2 and 2.7 kW/cm^2.

In the presented morphology results, the selected preloading stress values are also both the lowest and highest used values for all three specimen types. According to the rupture morphology, in the case of 1.5 kW/cm^2, when the preloading stress is lowest (46 MPa, 161 MPa, and 242 MPa), for all types of specimens the rupture morphology is a ')'-like shape in appearance, the edge is smooth, and the necking can be seen. When the preloading stress increases to maximum used values (97 MPa, 342 MPa, and 514 MPa), the necking extent reduces. In short, as the preloading stress increases, the degree of thermal softening before rupture decreases. When the preloaded stress increases to a certain extent, the phenomenon of thermal softening before rupture becomes less obvious.[16]

For the condition of 2.7 kW/cm^2, commonly the heat affected zone increases and local combustion effects are also visible. The increasing preloading stress does not produce any significant effects on rupture morphology during the highest used (2.7 kW/cm^2) laser power density. This behavior may be explained by that, under higher power densities and higher preloads, the relatively higher temperature and the higher heating rate do not allow heat accumulation and localized effects, and instead boost the thermal activation, dynamic softening, and failure processes.

The extent of damage to the laser irradiated specimens can be classified into three main categories depending on the laser power density and applied load level. The degree of damage to the tested specimens is identified as broken without obvious deformation, melt, and melt and deformed. From the observations, it is concluded that in general with the increase of preload level under constant laser power density, specimens

get fractured before reaching the melting point. While by the increase of laser power density under constant loading state, the melting phenomenon is favored. The degree of damage can be associated and justified from the corresponding failure temperature data provided in Section 3.3. Since comparatively higher failure temperatures were reported for Al-6061 type specimens, melting is observed up to higher preload levels.

3.4.1. Metallographs

The fracture surfaces of the specimens after tensile tests were examined through scanning electron microscope (SEM, FEI Quanta 250F). Some typical metallographs of fractured surfaces are presented in Fig. 12 to get a clearer picture of the fracture mechanism. Actually, metallographs corresponding to various experimental conditions were taken, but no significant difference in the fracture characterizing features was reported. Mainly, the appearance of dimples, dimple rupture, voids growth, and their coalescence was identified as fracture describing features. For the Al-1060 specimens in Fig. 12(a), primarily pillar-like structures having dimples and voids are observed. The specimens were fractured in the ductile mode because dimples are commonly assumed to be a feature of the ductile fracture mode.[24,25]

The formation of dimples arises from plastic strain during the growth and coalescence of microvoids.[26,27] During tensile loading, development of the dimples pattern is generally credited to local softening and structural disordering induced by applied stress and temperature rise.[28,29] For Al-6061 specimens in Fig. 12(b), rupture of dimples with tearing edges is found. Moreover, as discussed above, melting effects can be seen on the fractured surface. Whereas for the Al-7075 fractured surface in Fig. 12(c), the fracture mechanism seems to be turned toward brittleness. Briefly, for Al-6061 and Al-7075 specimens, the fracture evolution process follows the void nucleation, growth, and coalescence events through plastic flow. The initial voids tend to grow and expand under tensile loading with increased local stress concentration at higher laser power densities. The expanded induced defects act as favorable crack initiations and propagation sites, leading to relatively early failure of the specimens under higher preload and laser power densities. Moreover, for the Al-7075 specimen, the metallograph exhibits a dense net of shear bands or microcracks, which suggests localized brittle behavior.[30,31]

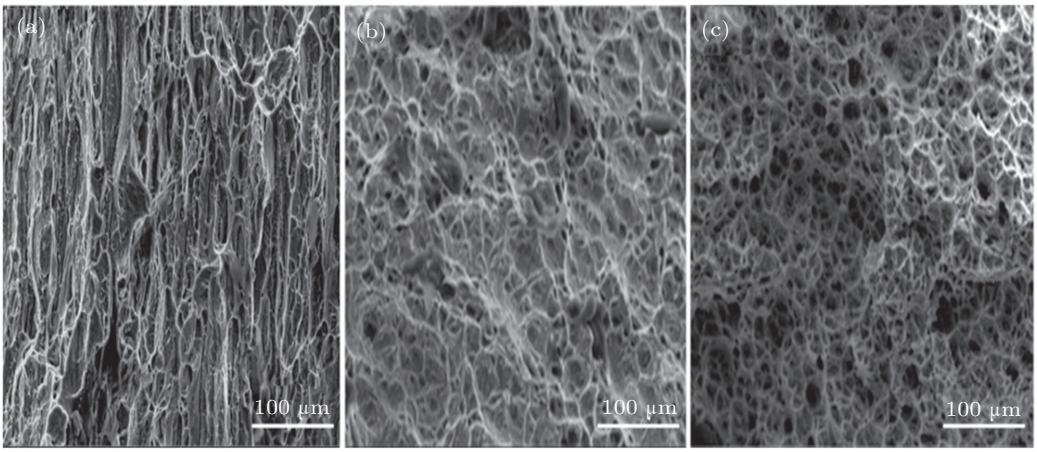


Fig. 12. Metallographs of the tested specimens fractured by 1.9 kW/cm^2 laser power density under different preloading values: (a) 80 MPa for Al-1060 specimen, (b) 282 MPa for the Al-6061 specimen, and (c) 423 MPa for the Al-7075 specimen.

3.5. Discussion

When the local region of the specimen is irradiated by the strong laser beam, the temperature in the laser irradiated region rises quickly and the thermal as well as mechanical properties of the specimens change dramatically, causing the specimen's softening, melting, and gasification spray. The thermal effects increase as the laser power density increases. For higher laser power densities, the absorption of laser energy increases, which results in temperature rise, material softening, and relatively rapid breakdown.[32] The mechanism behind this deformation is that the ultimate strength of the specimen significantly decreases with the increase of the exposure loading or temperature. In other words, it can be said that the load-bearing capacity of the material will be reduced under increased thermal or tensile loading.[3,33,34] The laser irradiated area gets into the plastic yield stage and with the increase of the exposure time the yield region expands to the specimen interior gradually, causing structural damage to the specimen.[32,34,35]

The experimental results reveal that depending on the laser power density level, material failure is followed by two kinds of thermal effects. Material removal due to ablation was found to dominate the response at high power densities, whereas thermal diffusion with the associated degradation of material properties was most apparent at lower laser power densities. When we compare failure time for different under-tested aluminum alloys under fixed tensile loading and fixed

laser power density, it is observed that Al-1060 type material takes the longest time to break down while Al-6061 type material takes the least time. Moreover, in comparison of the temperature rise rate for the three under-tested materials, it is found that, in general, with the increase of laser power density, the temperature rise rate for Al-6061 is highest and least for Al-7075 except for the maximum laser power density (shown in Figs. 8–10). The comparatively low temperatures in Al-7075 are attributed to the relative increase of micro defects in the preloaded material caused by local thermal inconsistency due to relatively low thermal conductivity value.

Mechanical property degradation during tensile loading and laser exposure can partly be examined through the strengthening mechanisms, which are alloy-dependent due to different chemical compositions and microstructural states from material processing (e.g. heat treatment and cold-work).[36] The Al-6061 and Al-7075 alloys are precipitation hardened, whose primary strengthening development is through precipitate growth under controlled heating (aging) to a required state. Combined (laser and tensile) loading and elevated temperature cause further precipitate growth (over aging) and strength reduction. The relatively long failure time of Al-7075 is possibly due to its high mechanical properties (tensile strength) as compared to Al-6061. The graphs of Al-1060 for both loading and laser powers exhibit the thermal diffusion and expansion before the complete failure. Comparing with the other two alloys, Al-1060 utilizes some energy and time in the localized thermal processes and the structure does not collapse immediately. This behavior is more obvious for low laser power densities and low load values. Due to the relatively high melting temperature, the Al-1060 alloy after the initial rise in temperature experiences the strain hardening well below the melting point during the plastic deformation. The combined effects of preload and thermal stress induced by the thermal expansion add to the specimen, which leads to local stress and shortens the failure time with the increase of power density or preloading. Studies considering only combined loading are not enough to fully understand the mechanical behavior. For complete characterization, one must consider the effect of heating as well as loading rate. The degradation of mechanical behavior under combined loading could not be explained only by thermal softening. High energy laser and the external load combination for the specimen is a complex process involving multiple physical fields simultaneously. Many aspects should be considered for more detailed investigation, such as the heat conduction process, the thermomechanical coupling theory, and the thermal elastic-plastic theory.

4. Conclusion

We attempted to explore the thermomechanical response of three different types of aluminum alloys under the combined tensile and laser loading. From the results, it is concluded that the load bearing capability of the under-tested specimens reduces due to thermal and mechanical effects caused by the laser irradiation to the preloaded material. The low loading values provide a long time for energy accumulation and high temperature boosts the thermal activation process of the alloys, accelerating the dislocation motion and annihilation which leads to dynamic softening. The fractured time was shortened with increasing either laser power density or preload value, while the failure temperature increases with increasing laser power density and decreases with the increase of preload. The preloads contribute significantly to the fracture of specimens under low laser power densities. For higher laser power densities, relatively imperceptible effects of preloading are noticed. The Al-1060 type material takes the longest time to break down and Al-6061 type material takes the least time. Fracture on a microscopic scale is predominantly ductile comprising micro-void nucleation, growth, and coalescence. Moreover, Al-1060 specimens behave plastically to some extent while Al-6061 and Al-7075 specimens experience catastrophic failure.

References

[1] Mabrouki T, Girardin F, Asad M and Rigal J F 2008 *Int. J. Mach. Tool. Manu.* **48** 1187
[2] Ma K, Wen H, Hu T, Topping T D, Isheim D, Seidman D N, Lavernia E J and Schoenung J M 2014 *Acta Mater.* **62** 141
[3] Lee H T and Shaue G H 1999 *Mater. Sci. Eng. A* **268** 154
[4] Imam M, Rahman M and Khan M 2015 *J. Eng. Sci. Tech.* **10** 730
[5] Li G R, Xue F, Wang H M, Zheng R, Zhu Y, Chu Q Z and Cheng J F 2016 *Chin. Phys. B* **25** 106201
[6] Konovalov S, Zagulyaev D, Chen X Z, Gromov V and Ivanov Y 2017 *Chin. Phys. B* **26** 126203
[7] Sathyajith S, Kalainathan S and Swaroop S 2013 *Opt. Laser Technol.* **45** 389
[8] Scintilla L D 2014 *Opt. Eng.* **53** 066113
[9] Medford J E and Gray P M 1980 *15th Thermophysics Conference*, July 14–16, 1980, Snowmass, USA, p. 1550
[10] Han W, Wang F, Zhou L D, Feng B, Jia H T, Li K Y, Xiang Y and Zheng W G 2012 *Chin. Phys. B* **21** 077901
[11] Cao Y, Zhao X and Shin Y C 2013 *J. Laser Appl.* **25** 032002
[12] Piehler T, Delucia F, Munson C, Homan B, Miziolek A and Mcnesby K 2005 *Appl. Optics* **44** 3654
[13] Irizalp S G, Saklakoglu N, Akman E and Demir A 2014 *Opt. Laser Technol.* **56** 273
[14] Hu H F, Ji Y, Hu Y, Ding X Y, Liu X W, Guo J H, Wang X L and Zhai H C 2011 *Chin. Phys. B* **20** 044204
[15] Gao X, Song X W and Lin J Q 2011 *Chin. Phys. B* **20** 024210
[16] Zhu Y, Ye X, Lin X, Wei C, Wang L and Cheng D 2012 *2nd International Symposium on Laser Interaction with Matter*, September 9–12, Xi'an, China, p. 8796
[17] Long L C, Wang T T and Liu L T 2015 *Mater. Res. Innov.* **19** 171
[18] Handbook A 1990 *ASM international* **2** 889
[19] Bowyer J, Luketa A, Gill W and Donaldson B 2011 *Fire Saf. Sci.* **10** 1151
[20] Boyer and Gall T L 1985 *American Society for Metals, Materials Park, OH*
[21] Jelani M, Li Z, Shen Z, Sardar M and Tabassum A 2016 *The 4th International Symposium on Laser Interaction with Matter (LIMIS 2016)*
[22] Ji L, Bin C, Quan Y, Ding-fei Z and Guo-zheng Q 2010 *Trans. Nonferrous Met. Soc. China* **20** 371
[23] Jiang J, Atkinson H V and Wang Y 2017 *J. Mater. Sci. Technol.* **33** 379
[24] Srivatsan T S, Sriram S, Veeraraghavan D and Vasudevan V 1997 *J. Mater. Sci.* **32** 2883

[25] Wojtaszek M, Sleboda T, Czulak A, Weber G and Hufenbach W 2013 *Arch. Metall. Mater.* **58** 1261
[26] Hassan S F, Zabiullah S, Al-Aqeeli N and Gupta M 2016 *J. Mater. Res.* **31** 100
[27] Irizalp S G and Saklakoglu N 2016 *Opt. Laser Eng.* **77** 183
[28] Joshi S S, Ghamarian I, Samimi P, Katakam S, Collins P C and Dahotre N B 2017 *Philos. Mag.* **97** 497
[29] Jelani M, Bashir S, Khaleeq-ur Rehman M, Ahamad R, ul-Haq F, Yousaf D, Akram M, Afzal N, Chaudhry M U, Mahmood K, Hayat A and Ahmad S 2013 *Eur. Phys. J. D* **67**
[30] Dalla Torre F H, Dubach A, Schällibaum J and Löffler J F 2008 *Acta Mater.* **56** 4635
[31] Li P H, Guo W G, Huang W D, Su Y, Lin X and Yuan K B 2015 *Mater. Sci. Eng. A* **647** 34
[32] Jelani M, Li Z, Shen Z and Sardar M 2017 *Appl. Sci.* **7** 464
[33] Chen B, Yuan Q and Luo J 2010 *Proceedings of the 12th International Conference on Aluminium Alloys* 2147
[34] Peng X H, Fan J, Yang Y, Chen Y and Yin Y 2003 *Int. J. Sol. Struct.* **40** 7385
[35] Mohsan J, Shazia B, Mahreen A, Daniel Y, Naveed A and Sajjad A 2014 *Phys. Scr.* **89** 025703
[36] Summers P T, Chen Y, Rippe C M, Allen B, Mouritz A P, Case S W and Lattimer B Y 2015 *Fire Sci. Rev.* **4** 1